Berger Scientfic Press

Study on flow field analysis and structure optimization in impeller of single-stage centrifugal compressor

Wei Luo*

Shenyang University of Technology, Liaoyang 111003, Liaoning, China

*Correspondence: luow0110@163.com

Abstract: Fluent's built-in Latin hypercube sampling is used to generate a sample space, a total of 32 design points, a high-precision calculation model needs to be generated by CFD, the design parameters and their value ranges are determined, the response surface is used to establish a surrogate model, and the particle swarm optimization algorithm is used to obtain the optimal design parameters of the impeller with the pressure ratio and efficiency of the single-stage centrifugal compressor as the optimization goal, so as to achieve better performance of the impeller of the single-stage centrifugal compressor.

Keywords: single-stage centrifugal compressor; impeller; responsive surface model; particle swarm optimization algorithm

1. Introduction

In this paper, the internal flow analysis and structural optimization of the impeller of a single-stage centrifugal compressor are studied, firstly, according to the optimized parameters, the design variables are determined, and the range of design variables is specified, so as to determine the parameter design table, which is usually automatically generated by the Fluent parameter design module after specifying the parameter range and the sampling method, and the sample space is generated by Fluent's built-in Latin hypercube sampling, with a total of 32 design points, and a high-precision calculation model needs to be generated by CFD[1]. After determining the sample space and CFD design points, the CFD high-precision model of each design point is automatically calculated by Fluent control, and the estimation of other sample points is generated through the response surface surrogate model algorithm, and the pressure ratio and efficiency of the single-stage centrifugal compressor are optimized by combining with the particle swarm optimization algorithm to achieve better performance of the single-stage centrifugal compressor impeller[2].

In order to verify that the optimized impeller has better performance, this paper also analyzes the flow field state inside the impeller before and after optimization, and verifies the feasibility of the optimization scheme[3].

2. Optimization method of impeller structure of single-stage centrifugal compressor

Figure 1 depicts a common CFD performance optimization process. Firstly, according to the optimized parameters, the design variables are determined, and the range of design variables is specified, so as to determine the parameter design table. The parametric design table is usually automatically generated by the Fluent parametric design module after specifying the parameter range and after the sampling method. Commonly used sampling methods include Latin hypercube sampling and optimal spatial filling[4]. The idea of both methods is to sample (calculate) from a limited number of sample points, and try to fill the entire sample space, so as to summarize the influence of design parameters

on the optimization goal to the greatest extent. In this study, Fluent's built-in Latin hyper-cube sampling was used to generate a sample space, with a total of 32 design points, which required high-precision calculation models to be generated by CFD, and their distribution is shown in **Table 1**[5].
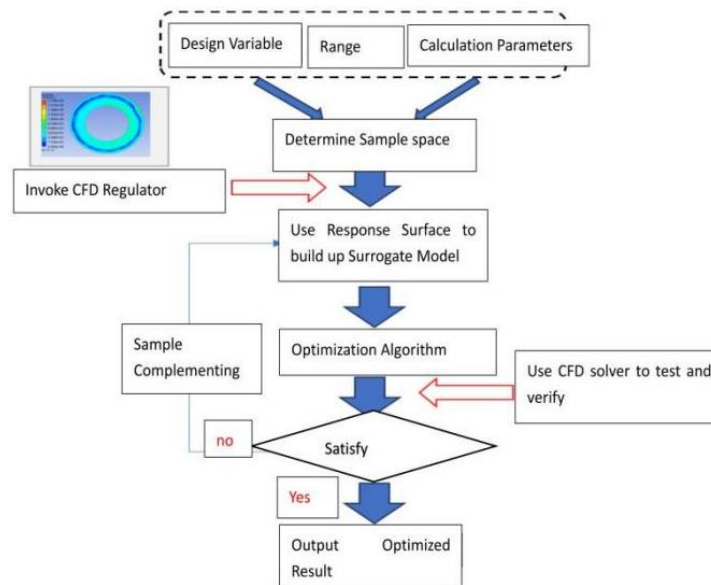
Figure 1. Schematic diagram of the CFD optimization process.

Table 1. Parametric design range

Impeller outlet width b2(mm)	[13,23]
Front cover arc radius r1 (mm)	[7,37]
Front cover straight section inclination a1 (°)	[2.4,11.6]
Radius of wheel arc r2(mm)	[38,65]
Wheel straight section inclination angle a2 (°)	[-0.8,5.4]
Blade inlet angle at the wheel seat $\alpha11$ (°)	[16,24]
Blade inlet angle at flange $\alpha12$ (°)	[10,15]
Blade exit angle at the wheel position $\alpha21$ (°)	[15,35]
Blade exit angle at rim $\alpha22$ (°)	15,35
Blade wrapping angle θ(°)	[40,70]

The schematic diagram of the main impeller front and rear cover profile variables is shown in **Figure 2**. The sample space is shown in **Table 2**.
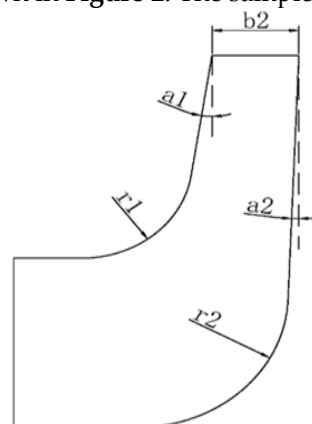
Figure 2. Schematic diagram of the profile variables of the front and rear cover plates of the impeller.

Table 2. The sample space.

numbering	b2	r1	a1	r2	a2	$\alpha 11$	$\alpha 12$	$\alpha 21$	$\alpha 22$	θ
1	21.1	19.5	2.90	62.7	4.50	19.6	14.9	34.8	25.1	43.5
2	22.1	8.50	8.70	38.0	2.70	16.8	10.9	16.3	24.8	64.4
3	14.3	34.1	2.80	50.5	5.00	24.0	11.3	33.8	32.5	49.7
4	22.1	35.3	3.10	49.5	3.50	18.7	12.0	15.4	22.1	47.4
5	19.3	21.7	7.20	50.4	2.80	18.4	10.4	28.7	24.0	50.3
6	14.0	21.7	3.30	58.8	4.30	16.5	13.4	30.7	34.3	51.3
7	15.8	17.1	9.90	46.7	4.60	18.4	12.0	25.7	15.8	56.4
8	18.5	34.0	9.90	59.2	5.30	16.4	14.9	32.7	34.5	56.9
9	22.6	18.1	9.00	50.7	-0.80	20.0	12.0	33.0	18.8	51.9
10	22.6	10.3	3.80	39.0	4.60	22.1	13.1	27.5	28.3	51.9
11	14.6	30.4	8.50	42.7	3.00	21.0	10.8	17.8	26.7	55.5
12	22.7	18.7	7.20	57.5	5.30	16.7	11.9	19.4	28.5	59.7
13	22.6	14.3	11.4	50.8	2.50	16.6	10.8	18.6	22.2	68.5
14	17.9	19.1	8.40	42.1	2.20	22.2	13.8	15.8	27.4	61.7
15	21.0	9.90	9.80	47.2	4.20	23.2	14.4	17.1	31.2	52.0
……	……	……	……	……	……	…….	……	……	……	……
141	21.5	12.5	4.70	52.4	4.70	20.4	11.4	29.3	26.5	66.0
142	19.2	14.2	4.50	40.4	-0.40	17.5	11.2	32.1	21.5	52.2
143	16.5	33.6	8.50	41.0	0.700	17.7	12.3	20.6	24.1	43.4
144	18.1	7.90	10.2	41.7	-0.50	16.6	11.1	29.6	29.3	53.3

After determining the sample space and CFD design points, the Fluent control automatically calculates the CFD high-precision model for each design point.

3. Theories of multi-objective optimization

For single-objective optimization problems, optimization can often be found through optimization algorithms, which is a process of continuously searching for the optimal solution of the optimization target through specific optimization algorithms and initial estimation. **Table 3** summarizes the common optimization algorithms.

Table 3. Common optimization algorithms

Optimization algorithms	Overview
Gradient descent method)	A commonly used optimization algorithm that continuously adjusts the parameters in an iterative manner to bring the objective function to a minimum or maximum value.
Stochastic gradient descent method	Only one sample is used per iteration to update the parameters, reducing the amount of computation
Genetic algorithms	The transmission algorithm simulates the process of biological evolution, searching for the optimal solution through selection, crossover, and mutation.
Particle swarm optimization algorithm	Simulate collective behaviors such as flocks of birds or fish, and search for optimal solutions through the transfer and updating of information between individuals.

In this study, the particle swarm optimization algorithm was adopted, and its implementation process is shown in **Figure 3**. Particle swarm optimization algorithm, and implementation process.
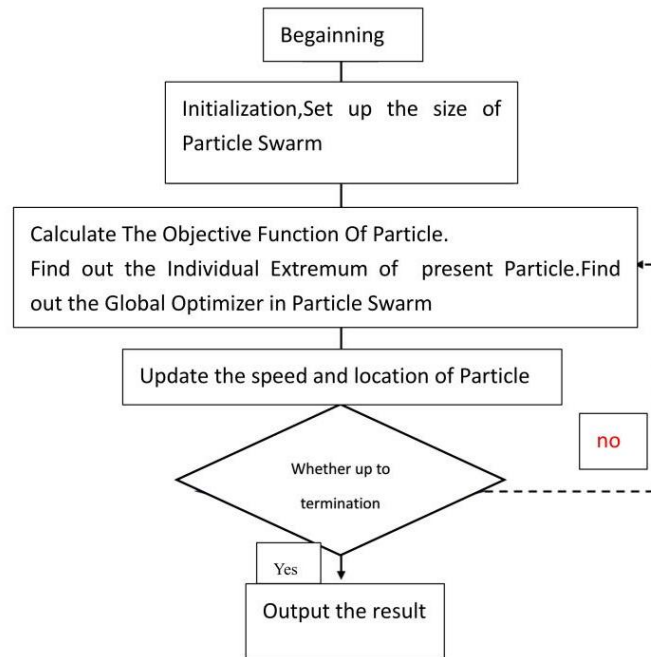
Figure 3. Particle swarm optimization algorithm, and implementation process.

4. Comparison of the structure of the impeller runner and the air outlet before and after optimization

4.1. Optimized the velocity distribution of the front and rear impeller flow channel speed outlets

Figure 4 illustrates the overall flow velocity distribution of the optimized front and rear impeller channels and outlets. As shown in **Figure 4(a)**, before optimization, the internal velocity of the internal channel of the outlet first increased and then decreased along the flow direction, and the flow uniformity was low. And the overall flow rate is lower than the optimized flow rate. Based on the connection of the impeller flow channel to the air outlet, it is inferred that the velocity of the air outlet close to the top of the impeller chamber increases the direct impact from the impeller chamber outlet. Near the impeller chamber, a smaller flow velocity is observed. The unevenness in the optimized compressor impeller flow channel is reduced and the symmetry is enhanced. In addition, the flow velocity in the outlet channel is uniform, except for the formation of a stable wall boundary layer near the wall, and its internal velocity is low, the flow velocity is relatively uniform in the range of 20 m/s – 40/ms.

(a)

(b)
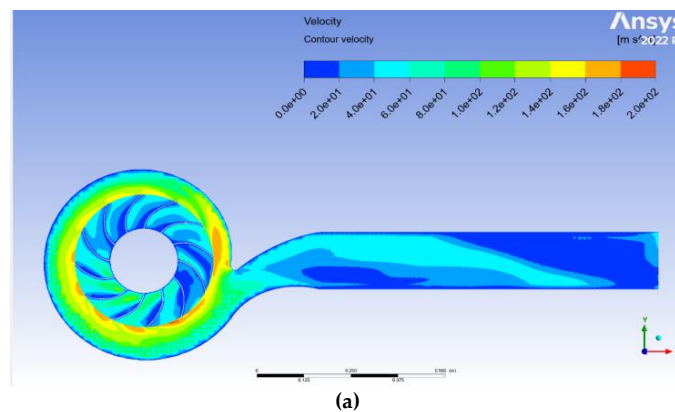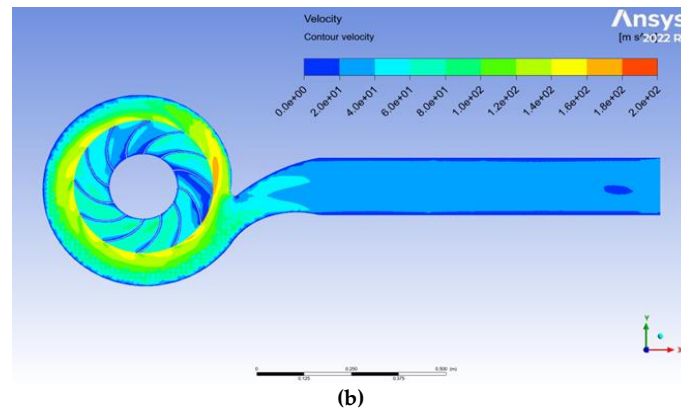
Figure 4. Before and after the improvement, the overall velocity distribution of the flow field of the impeller channel and the air outlet as a whole. **(a)** Before optimization; **(b)** After Optimization

Figure 5 shows the distribution of the velocity components U_x and U_y in the direction x and y in the direction of the flow before optimization in the impeller channel and outlet. As shown in the figure, in the vicinity of the impeller chamber and the outlet channel interface, U_x and U_y appear in an alternating positive and negative distribution, and on this surface, due to the improper design of the impeller chamber and the outlet channel interface, there is a reverse pressure gradient due to fluid congestion, resulting in the phenomenon of fluid separation. On the one hand, this reduces the compressor outgassing speed, and on the other hand, it exacerbates the unevenness of the fluid.

(a)

(b)
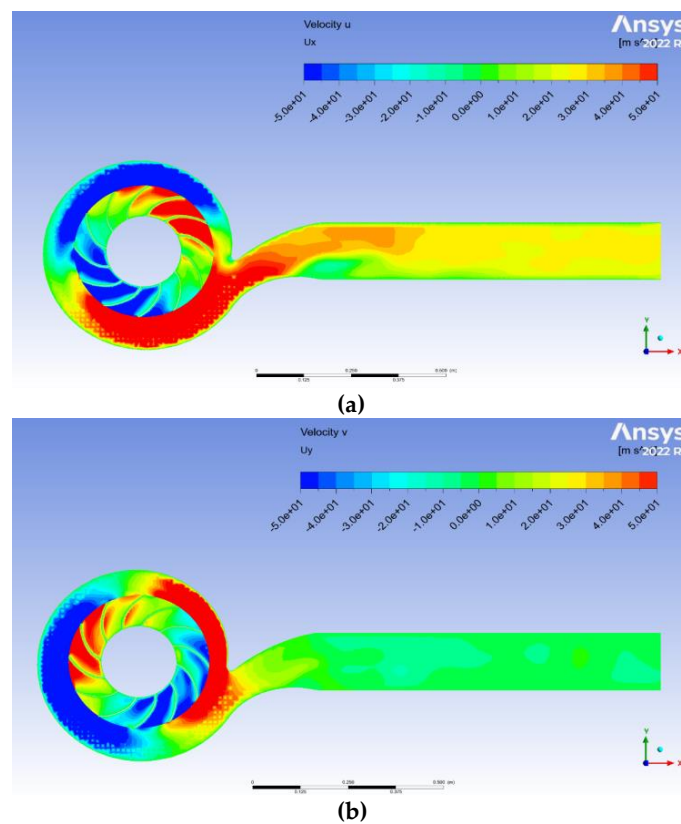
Figure 5. Before the improvement, the velocity components (U_x, U_y) in the x, y directions of the impeller runner and the air outlet were distributed. **(a)** Improved pre-U_x distribution; **(b)** Improved pre-U_y distribution

Figure 6 illustrates the distribution of the velocity components Ux and Uy in the direction x and y in the direction of the optimized flow in the impeller channel and outlet. As shown in **Figure 5(a)**, near the impeller chamber and outlet channel interfaces. In the horizontal direction, Ux flows uniformly, and the fluid velocity gradually weakens with the increase of the pipe diameter from the impeller chamber to the outlet channel, and its spatial distribution presents a slight imbalance. Then 4/5 of the way after the horizontal outlet, the horizontal flow rate quickly becomes homogeneous. **Figure 5(b)** shows the modified flow velocity from the impeller chamber to the vertical direction (y) within the outlet channel. Except at the interface near the impeller chamber, the velocity in the y direction is uniform and close to 0 at other locations, showing good flow characteristics.

(a)

(b)
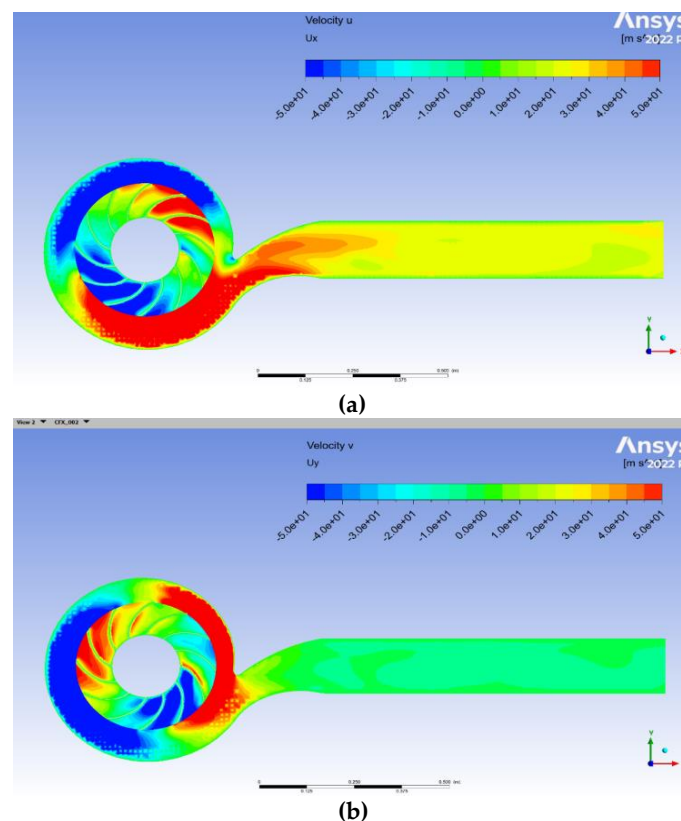
Figure 6. After the improvement, the velocity components (Ux, Uy) in the x, y direction (Ux, Uy) of the impeller flow channel and the air outlet are distributed. **(a)** Improved Ux distribution; **(b)** Improved Uy distribution

4.2. Optimized pressure distribution at the front and rear impeller flow channel speeds

Figure 7 illustrates the overall pressure distribution between the front and rear impeller channels and outlets at the optimized front. As shown in the figure, there is a large pressure gradient at the interface between the impeller chamber and the outlet channel before the improvement, and the gradient direction presents a large angle with the horizontal outlet. This indicates that the pipe diameter of the impeller chamber outlet is not properly designed, and a part of the air flow hits the wall of the outlet pipe, forming a lateral backpressure gradient, which induces the separation vortex at

the interface (**Figure 4**, **Figure 5**). On the contrary, at the improved interface, although the pressure gradient is still large, its direction is roughly parallel to the direction of the flow field, the pressure gradient comes from the driving effect of the impeller, the wall at the interface does not cause pressure loss, and the geometric arrangement of the compression turbine is more reasonable.

(a)

(b)
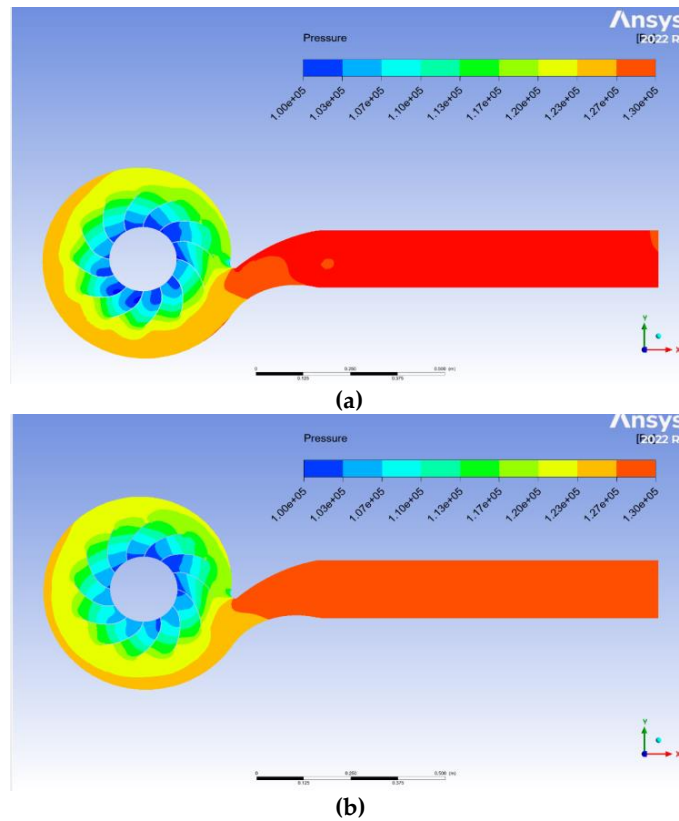
Figure 7. Before and after the inlet, the pressure distribution of the impeller channel and the air outlet. **(a)** Improved pre-pressure distribution; **(b)** Improved pressure distribution

4.3 Optimized the turbulence of the front and rear impeller runners

The degree of disturbance of the fluid can be expressed by the intensity of the turbulence. At the same time, in numerical calculations, the turbulent viscosity also reflects the degree of fluid disorder to a certain extent. However, the two emphases are different, the turbulence intensity focuses on the existing energy of the turbulent flow, and the turbulent energy is converted into heat energy through small-scale dissipation, so the turbulent viscosity can reflect the dissipation of turbulence to a certain extent. In the fully developed turbulent flow, the turbulent dissipation and turbulent generation are balanced, so the turbulent viscosity can reflect the turbulent generation to a certain extent in the steady-state calculation in this study.

Figure 8 shows the turbulence intensity distribution of the impeller channel and outlet before and after the improvement. Due to the turbulence of the impeller and the inner height, the turbulence at the air outlet is not obvious. However, it can still be seen that for the previous improvement, the velocity gradient increased due to the impact of the fluid on the wall near the impeller chamber on the upper side of the air outlet channel, thereby increasing the turbulent energy (intensity). At the same time, there is a local extreme value in the turbulence at the lower part of the outlet channel near the impeller chamber, which may be due to the additional turbulent energy brought by the local return transfer upstream, or the increased turbulence generation rate at this location. This needs to be further studied.

(a)

(b)
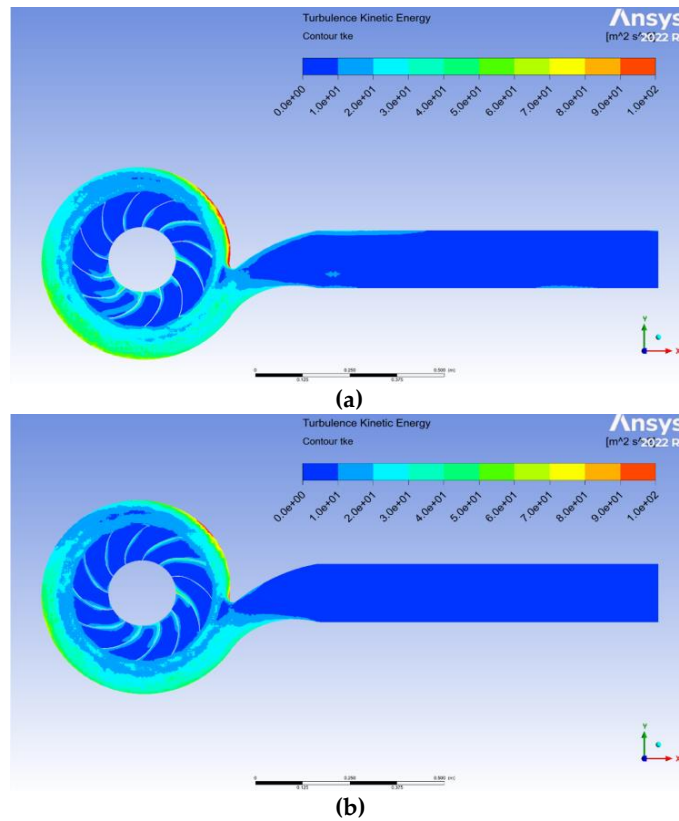
Figure 8. Improved turbulence intensity distribution of impeller runner and outlet before and after. **(a)** Before improvement; **(b)** Improved

The turbulent viscosity reflects the dissipation of the turbulent value to a certain extent. In the impeller chamber, due to the forced rotation, the fluid velocity gradient is large, and the turbulent generation rate is high, which is greater than the turbulent dissipation, so after leaving the impeller chamber, the turbulent energy gradually weakens as the turbulence generation decreases (**Figure 8**).

(a)

(b)
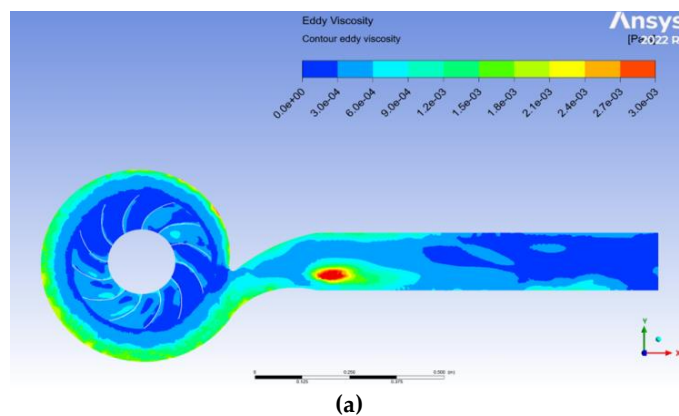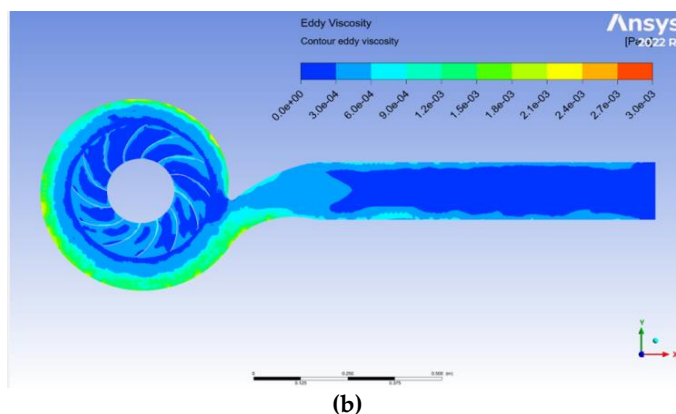
Figure 9. Turbulent viscosity distribution of impeller runner and outlet before and after improvement. **(a)** Before improvement; **(b)** Improved

Figure 9 shows the turbulent viscosity distribution of the impeller channel and outlet before and after the inlet. In places where the turbulent flow energy is high, the turbulent dissipation is enhanced, so the turbulent viscosity is high, and the turbulent viscosity shows a high similarity with the turbulent flow energy in the impeller chamber.

It is worth noting that before the improvement, a local extreme value of turbulent energy appeared on the upper side of the air outlet channel near the lower part of the impeller chamber (**Figure 10**), and correspondingly, the turbulent dissipation was also enhanced at the changed position. Due to the unreasonable design of the internal channel, the fluid at the outlet of the impeller chamber directly hits the wall, and the strong swirl flow caused by the strong swirl flow converts the average kinetic energy of the fluid flow into turbulent energy. The increased turbulent energy in turn increases turbulent dissipation, resulting in an increase in turbulent viscosity. As a result, the kinetic energy of the fluid is lost, the outlet velocity is reduced, and the internal energy (temperature) is increased.

Figure 10 and **Figure 11** show the flow field distribution inside the impeller chamber at different locations (z=0.02m, 0.03m, 0.04m, and 0.05m), respectively. The compressor impeller is the core component of the compressor, and during the rotation of the blades driven by external power (such as a motor or engine), the compressor impeller interacts with the surrounding fluid, and the blades push and accelerate the fluid. The fluid forms a change in velocity and pressure on the blades. As the fluid is further pushed and accelerated through the blades, its kinetic energy is converted into static pressure energy, thus achieving the compression of the fluid. Therefore, at the position close to the inlet chamber (z=0.02m), the fluid flow velocity is driven by the impeller blades, which increases significantly, and as the fluid flows downstream (z=0.03-0.05m), its kinetic energy is gradually converted into static pressure energy, and the kinetic energy decreases and the fluid velocity decreases.

z=0.02m

z=0.03m
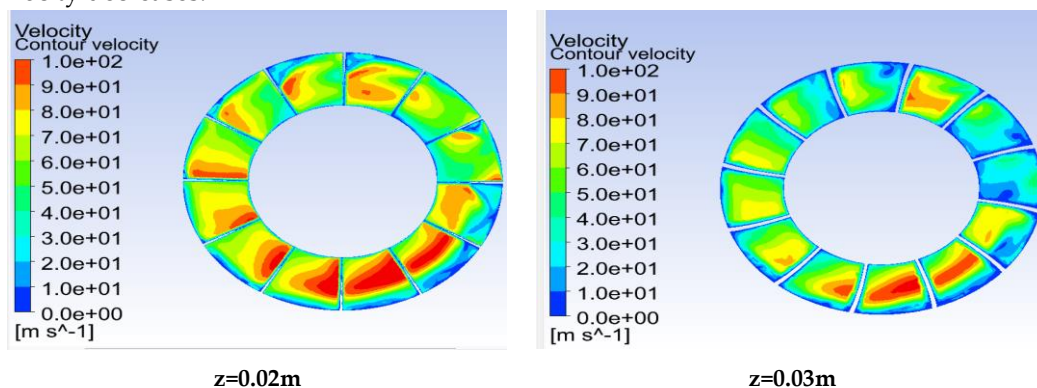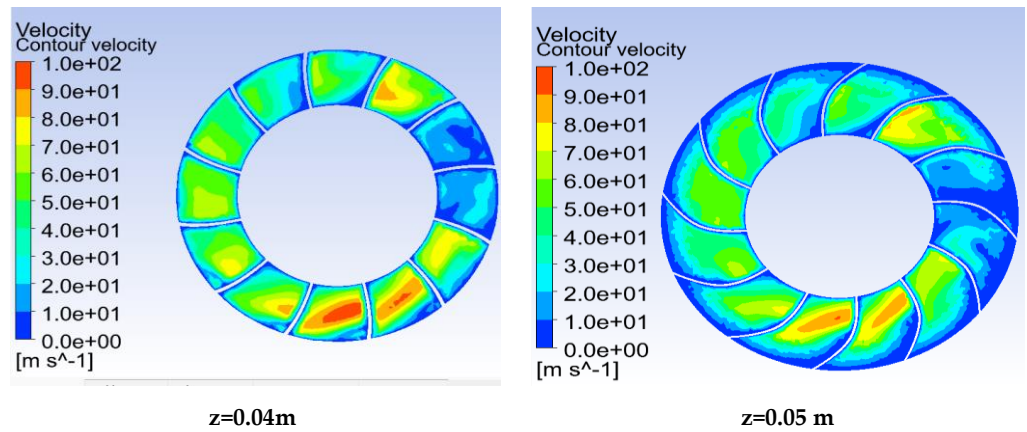
Figure 10. Detailed velocity distribution inside the impeller chamber before improvement.
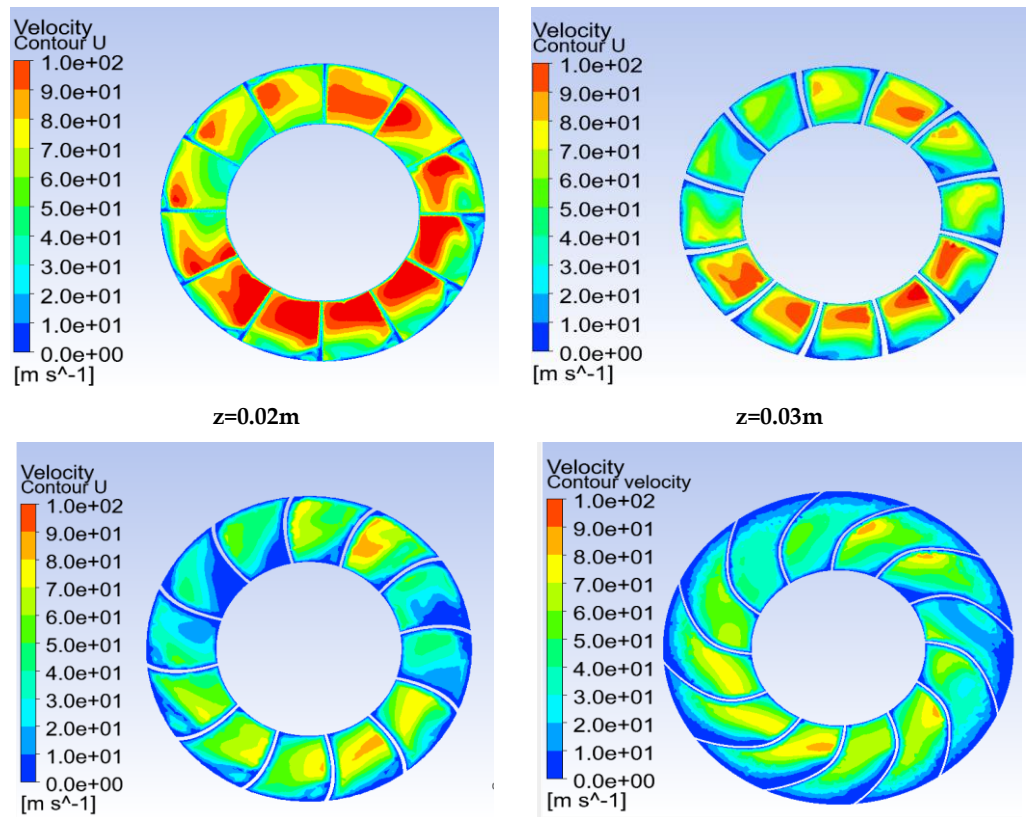
Figure 11. Detailed velocity distribution inside the impeller chamber after improvement.

Compared with the pre-improvement period, the improved impeller blade near the air intake chamber (z=0.02m) enhances the fluid coupling and increases the driving capacity, so the flow velocity is greatly increased compared with the pre-improvement period, which is conducive to the further conversion of kinetic energy into static pressure energy and improves the efficiency and pressure ratio of the compressor. At the same time, as the gas moves from the impeller chamber to the outlet, the uniformity of the air flow rate is improved in the optimized chamber, which helps to reduce the pressure loss inside the chamber.

Figure 12 shows the static pressure distribution on the surface of the impeller blades before and after the improvement. As shown in the figure, the pressure on the surface of the impeller gradually increases outward along the radius, which is due to the fact that

the acceleration is proportional to the radius, and when the air of similar velocity enters from the air intake, it is accelerated to different speeds in the same time, and the gas acceleration on the outside is large, requiring the impeller blade to exert more pressure. It is worth noting that the uniform distribution of pressure is conducive to reducing the vibration of the impeller during operation, reducing the operating noise of the compressor and prolonging the life of the compressor. Compared with the previous improvement, the surface static pressure of the improved compressor impeller blade is significantly increased, which indicates that the interaction between the impeller blade and the fluid is significantly enhanced at the same speed, which increases the acceleration and compression effect on the fluid. This coincides with the previous time when the fluid had greater velocity (kinetic energy) in the modified impeller chamber. At the same time, the improved impeller surface static pressure distribution is relatively uniform, which is conducive to uniform acceleration fluid, reduces the loss of local kinetic energy and pressure energy, improves the pressure ratio and efficiency, and also increases the mechanical life and reduces the operating noise.

(a)

(b)
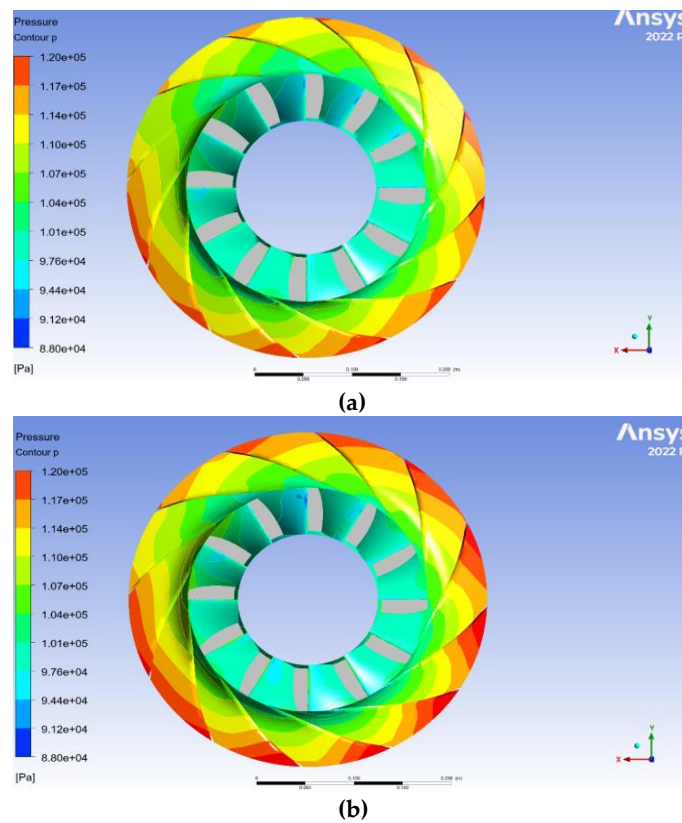
Figure 12. Before and after the improvement, the pressure distribution on the blade surface inside the impeller chamber. **(a)** Before improvement; **(b)** Improved

Figure 13 and **Figure 14** show the detailed turbulent energy distribution of different sections inside the impeller chamber before and after the improvement. Ideally, the turbulence intensity should be distributed as evenly as possible inside the impeller chamber. This ensures a stable flow of fluid inside the impeller chamber and maximizes the performance and efficiency of the impeller. And near the wall of the impeller blades, the turbulence intensity should be large enough to facilitate the momentum exchange and energy transfer between the impeller and the fluid. Before the improvement, the distribution of the impeller and internal turbulence was relatively disordered, and the internal turbulence degree was high, which increased the dissipation rate of momentum and kinetic energy. After the improvement, the interior of the impeller chamber presents a more ideal

state, that is, the turbulent flow energy is higher near the impeller blades, which increases the coupling between the impeller blades and the fluid. In the core region of the fluid, the turbulent flow energy decreases rapidly, the distribution is relatively uniform, and the overall value is smaller than before the improvement.

Figure 14 and **Figure 15** show the detailed turbulent viscosity distribution of different sections inside the impeller chamber before and after the improvement. The turbulent viscosity mainly shows the dissipation velocity of the turbulent flow, which is directly proportional to the turbulence intensity when the turbulence is stable. As can be shown, the distribution of turbulent viscosity is similar to that of turbulent intensity in the impeller chamber. Before the improvement, the turbulent viscosity was high and the distribution was uneven, and after the improvement, the viscosity decreased to a certain extent, and the high viscosity was mainly concentrated in the near-wall area.

z=0.02m   z=0.03m

z=0.04m   z=0.05m
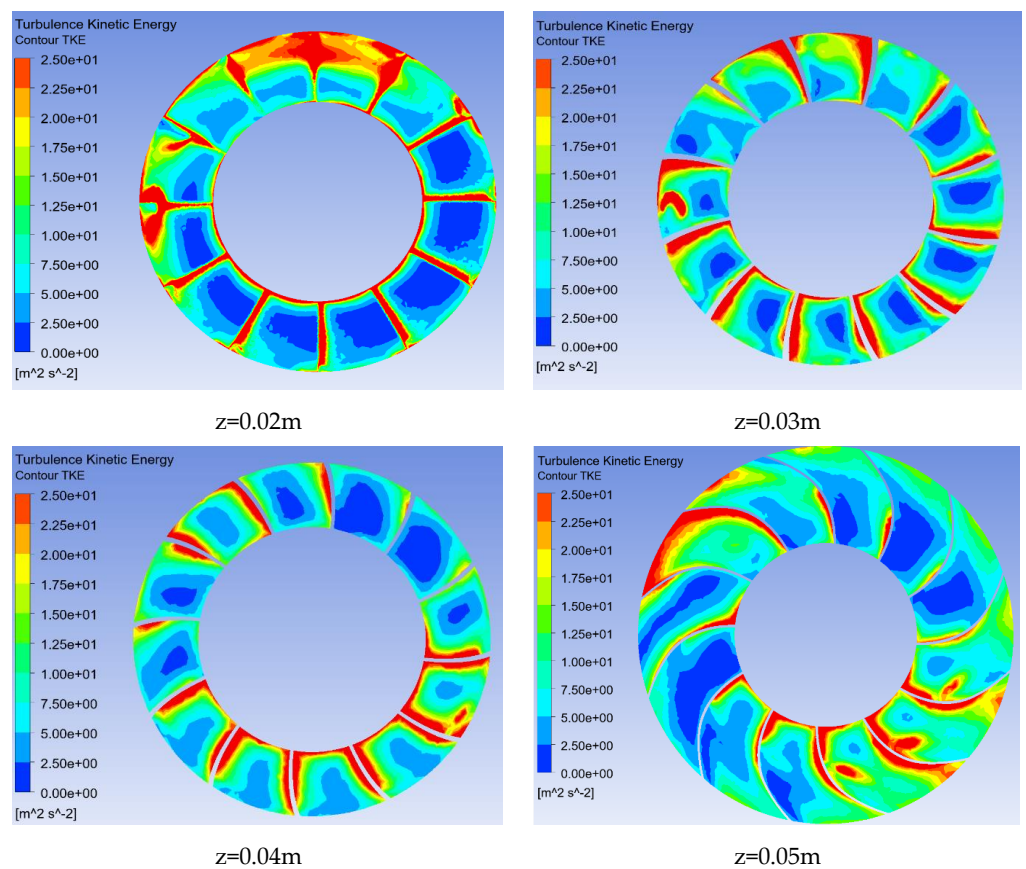
Figure 13. Before the improvement, the turbulent energy distribution inside the impeller chamber was detailed

z=0.02m   z=0.03m

z=0.04m   z=0.05m
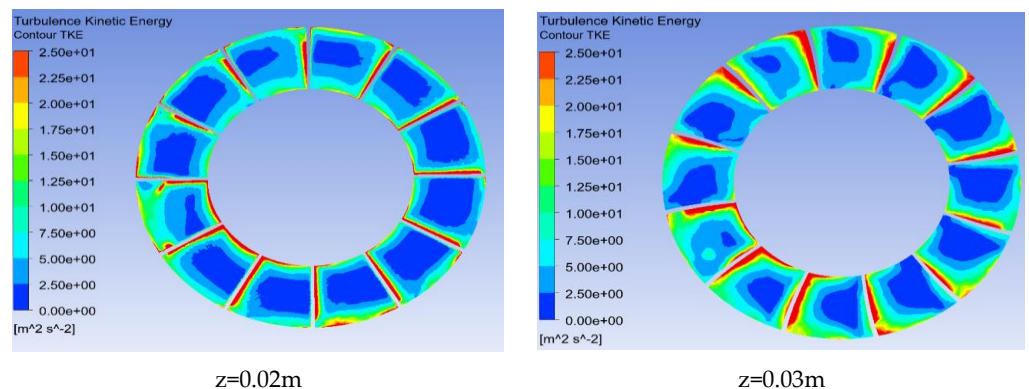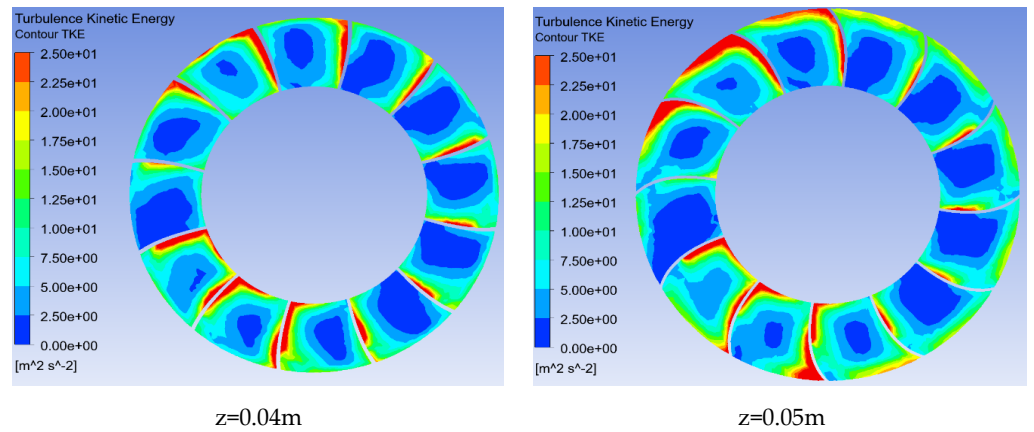
Figure 14. After the improvement, the turbulent energy distribution inside the impeller chamber is detailed.

z=0.02m   z=0.03m

z=0.04m   z=0.05m
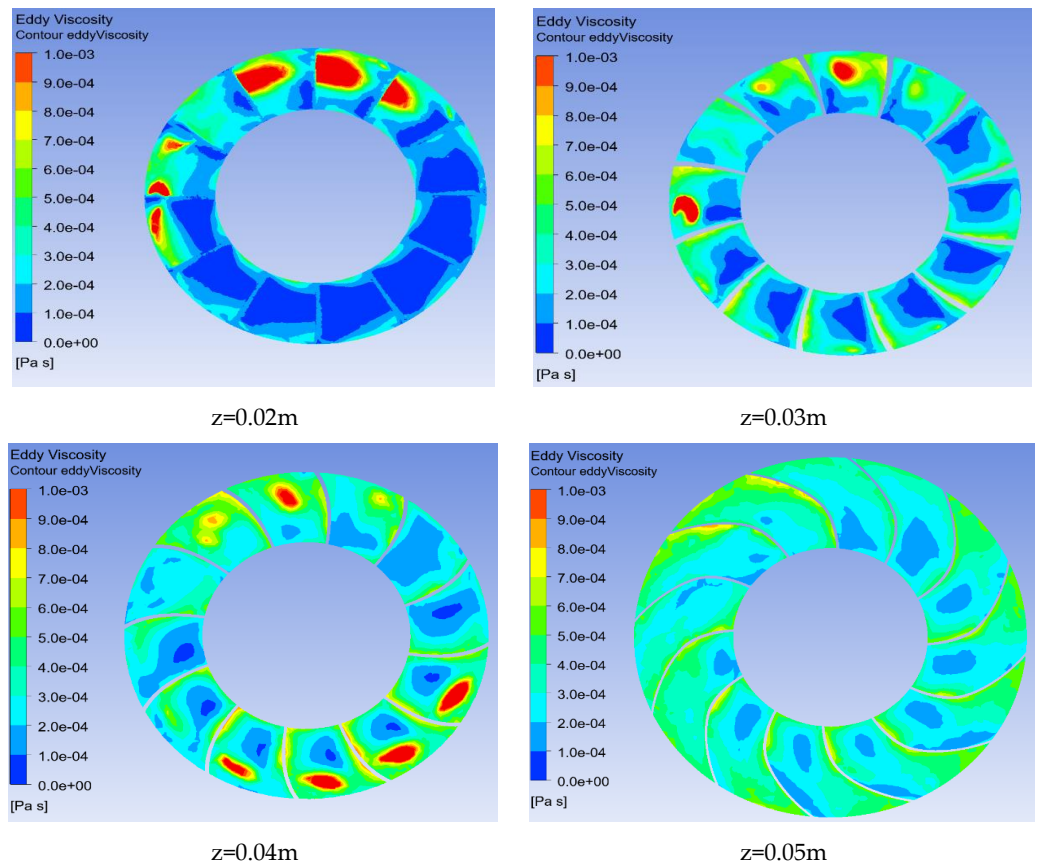
Figure 15. Before the improvement, the turbulent viscosity distribution inside the impeller chamber was detailed.

z=0.02m

z=0.03m

z=0.04m

z=0.05m
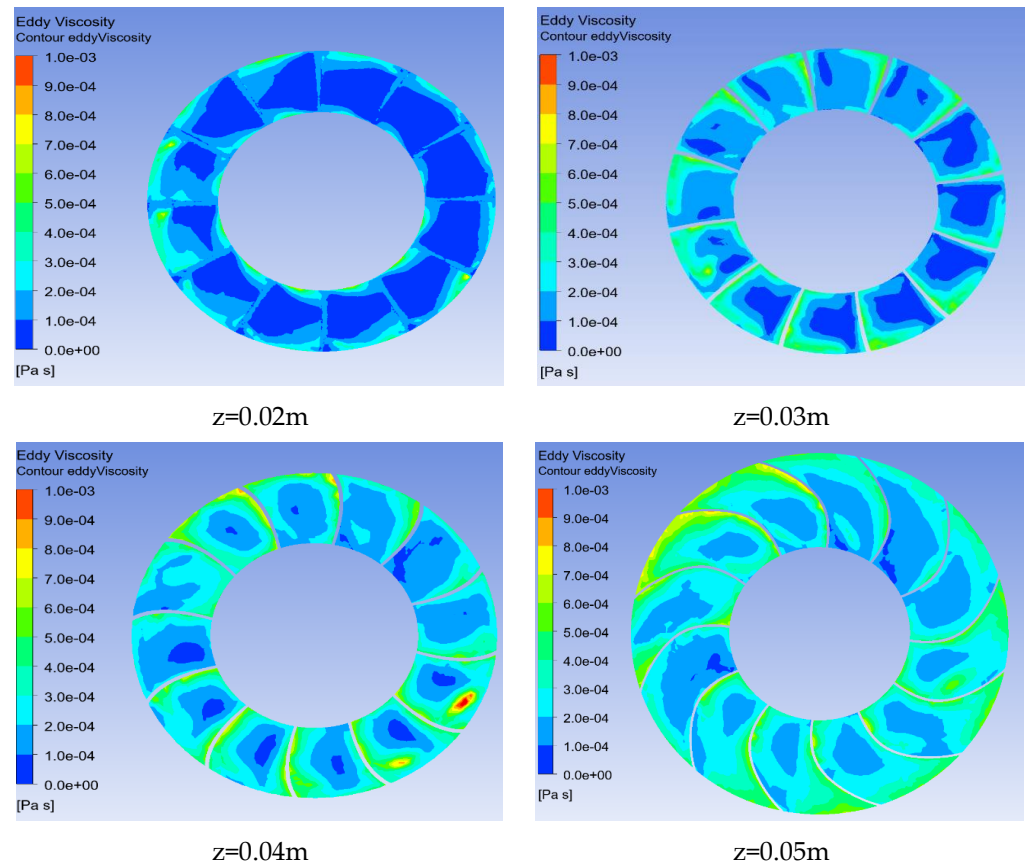
Figure 16. After improvement, the turbulent viscosity distribution inside the impeller chamber is detailed

5. Conclusions

This paper analyzes the flow situation inside the impeller chamber, especially the direct effect of the impeller disc on the flow field inside the impeller chamber, which directly affects the compressor efficiency efficiency and pressure ratio. The impeller blades rotate at high speed inside the impeller, driving the air into the impeller to move, resulting in an unstable flow (turbulence) of the fluid on the surface of the impeller blades, resulting in drastic changes in fluid velocity and pressure. Turbulence has an important impact on the performance and vibration of the impeller, and reasonable turbulence control and optimization design are required. The article also provides a detailed study of the interior of the impeller machine. ResultsOn the surface, the static pressure on the surface of the impeller increases significantly after optimization, indicating that the coupling between the impeller and the fluid is close, and the energy and momentum transfer are increased, which is conducive to improving the efficiency and pressure ratio. At the same time, the turbulence distribution in the optimized impeller chamber is ideal. Firstly, the turbulence intensity near the impeller blade is significantly enhanced, which is conducive to the momentum exchange between the blade and the fluid as a whole. Secondly, in the core region of the fluid, the turbulent energy and turbulent viscosity are larger, which is conducive to the maintenance of energy. At the same time, the speed, pressure, symmetry and uniformity of turbulence intensity in the impeller chamber after optimization are greatly improved, which is conducive to reducing blade vibration, suppressing fluid noise and improving mechanical service life.

References

1. Chen, D., Wu, H., Zhang, C. Analysis and research on main aerodynamic design parameters for impeller of centrifugal compressor. Chinese Journal of Turbomachinery, 2006, 3:1-4. https://doi.org/10.3969/j.issn.1006-8155.2006.03.001
2. Chen, X., Miao, Y. The compuation of intertnal flow fields in centrifugal compressor impellers. Journal of Engineering Thermophysics, 1992, 18(3): 277-281.
3. Cortés, O., Urquiza, G., Hernández, J. A. Optimization of operating conditions for compressor performance by means of neural network inverse. Applied Energy, 2009, 86(11): 2487-2493. https://doi.org/10.1016/j.apenergy.2009.03.001
4. Bacak, A., Çolak, A. B., Dalkılıç, A. S. Investigating hermetic reciprocating compressor performance by using various machine learning methods. Proceedings of the Institution of Mechanical Engineers, Part C: Journal of Mechanical Engineering Science, 2023, 09544062231213276. https://doi.org/10.1177/09544062231213276
5. Wu, D., Asl, B. B., Razban, A., Chen, J. Air compressor load forecasting using artificial neural network. Expert Systems with Applications, 2021, 168, 114209. https://doi.org/10.1016/j.eswa.2020.114209